European Conference on Optical Communication (ECOC) 2022 © Optica Publishing Group 2022

3-Dimensional Visible Light Positioning (VLP) Using Two-Stage Neural Network (TSNN) and Signal-Strength-Enhancement (SSE) to Mitigate Light Non-Overlapping Regions

Li-Sheng Hsu(1, 2), Chi-Wai Chow(1, 2, *), Yang Liu(3), Yun-Han Chang(1, 2), Deng-Cheng Tsai (1, 2), Tun-Yao Hung(1, 2), Yuan-Zeng Lin(1, 2), Yin-He Jian(1, 2) and Chien-Hung Yeh(4)

(1)Department of Photonics, National Yang Ming Chiao Tung University, Hsinchu 30010, Taiwan
(2)Department of Photonics, National Chiao Tung University, Hsinchu 30010, Taiwan
(3)Philips Electronics Ltd., N.T., Hong Kong
(4)Department of Photonics, Feng Chia University, Seatwen, Taichung 40724, Taiwan
*Corresponding author email: cwchow@nycu.edu.tw

Abstract *We propose and present the first demonstration of a 3-D visible-light-positioning (VLP) utilizing Two-Stage-Neural-Network (TSNN) and Signal-Strength-Enhancement (SSE) to mitigate the light-non-overlapping-regions. In a practical room of 200×150×300 cm^3, the average errors are <9 cm.*

Introduction

The recent development of Internet-of-Things (IOT), wireless sensor networks, Virtual Reality/Augmented Reality (VR/AR) applications require high precision and accurate indoor positioning. Recently, visible light communication (VLC) and light fidelity (Li-Fi) systems have been commercialized [1-5], and these VLC systems are also potential candidates for indoor visible light positioning (VLP) [6]. Different VLP methods have been proposed, such as using proximity [7], time-of-arrival (TOA)/time-difference-of-arrival (TDOA) [8], angle-of-arrival (AOA) [9], and received-signal-strength (RSS) [10]. Among these VLP methods, RSS method is simple and accurate. As the received optical power has an inverse relationship with the distance between light emitting diode (LED) transmitter (Tx) and receiver (Rx), positioning can be realized by analyzing the received optical power from several LEDs with different identifier (ID) or carrier frequencies. Besides, to further reduce the positioning error, machine learning (ML) algorithms were utilized. Recently, a 3D VLP system using artificial neural network (ANN) and hybrid RSS/phase-differences-of-arrival (PDOA) was proposed having 12 cm average error; however, only simulation was provided [11]. Experimental 3D VLP systems using deep learning (DL) [12] and ANN [13] were also proposed; however, the positioing unit cells are small and impractical.

In this work, we propose and present the first demonstration up to the authors' knowledge a 3D RSS VLP system utilizing Two-Stage Neural Network (TSNN) with Signal-Strength-Enhancement (SSE) to mitigate the light non-overlapping regions caused by the finite field-of-view (FOV) of LEDs at different height. The experimental results show that in a practical room of 200 × 150 × 300 cm^3, the average positioning error in *z*- and *xy*-directions are 8.80 and 8.91 cm respectively. The errors in *z*- and *xy*-directions are reduced by 27.9% and 37.8% respectively when compared with the one-stage neural network without SSE.

3D VLP TSNN Algorithm and Experiment

Fig. 1(a) shows the photo and architecture of the proposed 3D VLP system. The positioning unit cell contains 4 LEDs (TOA® LDL030C), and each has an output power of 13 W. Each LED is encoded by a unique Manchester-coded ID at data rate of 3.125 kbit/s and upconverted to different specific RF carrier frequency (i.e. 47 kHz, 59 kHz, 83 kHz, or 101 kHz) as also illustrated in Fig. 1(a). The odd frequencies used are to avoid harmonic frequency overlapping. The vertical distance of the room is ~ 300 cm. A photodiode (PD) is connected to a real-time-oscilloscope (RTO, PicoTechnology® ps5432d) to collect real-time RSS data. They are mounted on an autonomous mobile robot (AMR). Fig. 1(b) shows the top-view of the VLP using cell; illustrating the training, testing and LED locations. In this practical experimental test-bed, the unit cell is not a perfect rectangle, and the size is about 155 cm × 200 cm. We collect the training and testing data from 3 layers at different heights, and the distances are 250, 225, and 200 cm away from the LED plane (i.e. ceiling). For each layer, we measure 112 location points, of which 58 and 54 location points are for training and testing respectively. Each point is measured 20 times. Hence, the training set has 3480 data (58 locations × 20 times × 3 layers), and the testing set has 3240 data (54 locations × 20 times × 3 layers).

978-1-6654-3868-1/21/$31.00 ©2021 IEEE

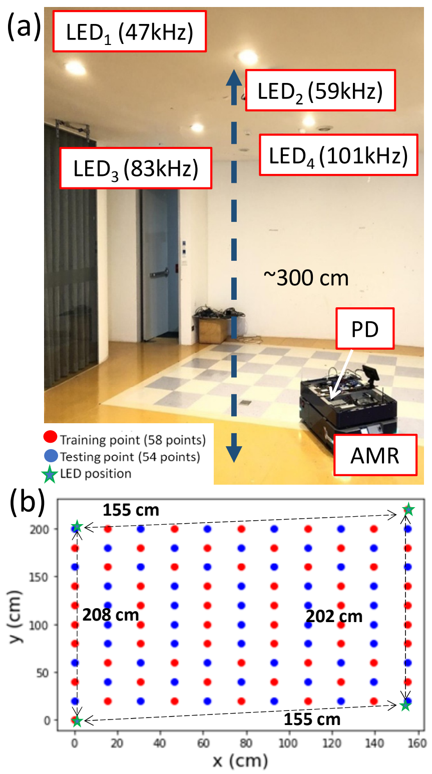

Fig. 1: (a) Photo of the VLP test-bed. PD: photo-detector; AMR: autonomous mobile robot. (b) Top-view of the VLP layer; illustrating the training, testing and LED locations.

It is generally think that VLP performance will decrease when the distance between Tx and Rx increases due to the reduction of optical signal-to-noise ratio (SNR). However, due to the finite FOV of LEDs, light non-overlapping areas are created as depicted in Fig. 2(a). These light non-overlapping regions will produce high positioning error since no light is detected. Figs. 2(b) and (c) are the top-views of 200 and 225 cm Rx planes away from the LED plane respectively. We can observe that light non-overlapping region (i.e. gray area) is bigger at the 200 cm plane.

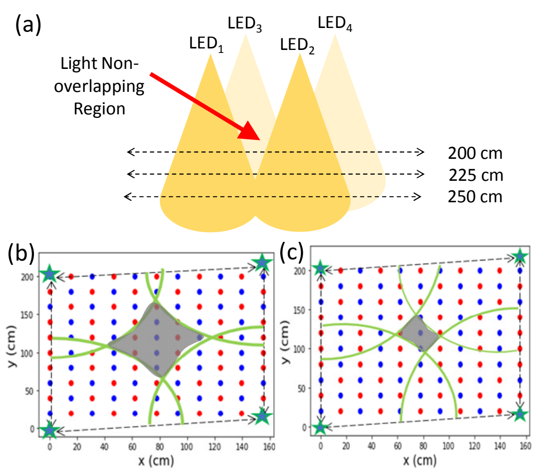

Fig. 2: (a) Schematic illustrating the LEDs, and light non-overlapping regions. Top-view of the (b) 200 cm (c) 225 cm Rx plane.

Fig. 3(a) shows the flow diagram of TSNN model. In the first stage of the TSNN, the 4 RSS data and total RF signal strength are used as the input data. Then, data pre-processing, including Z-score normalization and extanding cross-term are performed. Hence, the 4 RSS data will become 14 RSS data with cross-terms [p_1, p_2, p_3, p_4, p_3p_4, ... p_3, p_4^2]. Then the data is divided into training and testing set based on their locations illustrated in Fig. 1(b). Fig. 3(b) shows the architecture of NN model 1. It has 5 layers, including 1 input, 1 output and 3 hidden layers. There are 15 nodes at the input layer (i.e. labeled as input(,15)) representing the 14 RSS features and 1 total RF signal strength. The nodes of 3 hidden layers are 32, 16 and 8, respectively, and they are fully connected (FC). The activation function is Rectified Linear Unit (ReLU). The loss function and optimizer used are mean-square-error (MSE) and Adam respectively, and the training epochs is 400. The output layer in the first stage of the TSNN predicts the *z* coordinate, and we use dropout layer (rate = 0.3) to avoid over-fitting. After the prediction of the *z* coordinate, the proposed SSE (i.e. blue block in Fig. 3(a)) is executed. The detail of the SSE will be discussed later. The data will be proceeded by the second stage of the TSNN, with the NN model 2 illustrated in Fig. 3(b). The nodes of input layer are 15, which consist of the 14 RSS features with cross-terms and the z coordinate from the first stage. The standard deviation in Gaussian noise layer is 0.15, and the nodes of output layers are 2 which represent the predicted *x* and *y* coordinates. The remaining parameters of second stage TSNN model, such as loss function and optimizer are same as the first stage TSNN.

Here, we discuss the proposed SSE. As mentioned above, at the 225 and 200 cm Rx planes, there are light non-overlapping regions. The SSE process is to compensate the light non-overlapping regions based on the ratio of other illuminated region, as shown in Eq. (1),

$$RSS_{enhanced} = RSS_{original} + \frac{(h_{std} - h_{target})\tan\theta}{h_{std}\tan\theta}\alpha \quad (1)$$

where h_{std} is the height of the standard layer, which is set at the 250 cm Rx plane since there is no light non-overlapping region, and h_{target} is the height of the target layer (i.e. 225 or 200 cm). θ is the divergence angle of the LED lamp, which is set at 32^o based on our measurement. By multiplying the tanθ and the height, we can obtain the size of the illuminated region of the LED lamp at this height which is the denominator. For the numerator, we can calculate the extent to which the LED illuminated region is reduced due to the height. After knowing the reduced ratio at different heights, we will multiply an α to control the compensation level of the RSS value.

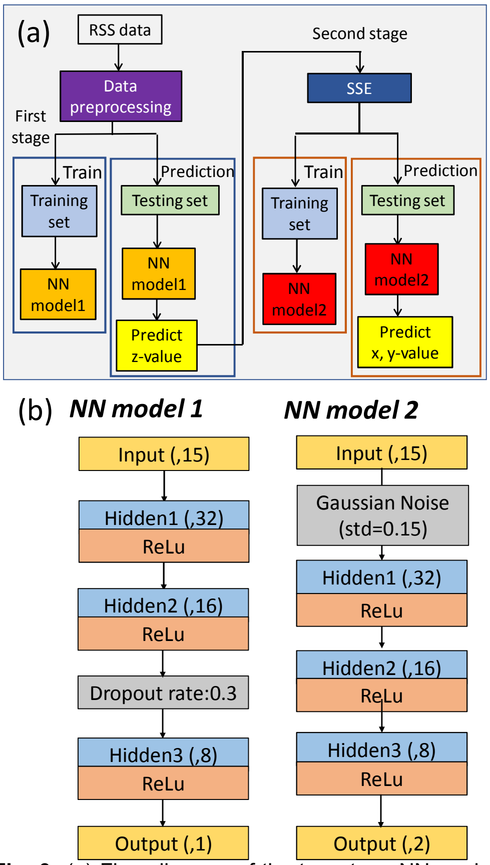

Fig. 3: (a) Flow diagram of the two stage NN model. (b) The structure of NN model 1&2 inside the TSNN.

Results and Discussion

When one stage NN model is employed, the mean and standard deviation (SD) of errors for the testing data set in the vertical direction (*z*-direction) are 12.20 and 9.92 cm, respectively. The mean and SD errors in the horizontal direction (*xy*-direction) are 14.33 and 8.92 cm, respectively. Figs. 4(a)-(c) show the average error distributions of the testing data set at different Rx planes. The red dots are the location of the testing points. The radius and color of circle is the average error in *xy*- and *z*-directions respectively. We can observe that when the height increases, the average error in the *xy*-direction is larger. When the proposed TSNN model with SSE is employed, the mean and SD errors for the testing data set in *z*-direction are 8.8 and 9.9 cm, respectively. The mean and SD errors and for *xy*-direction are 8.91 and 5.81 cm, respectively. We can observe in Figs. 4(a)-(c) that when using the TSNN with SSE, the positioning error as well as the error variation can be significantly reduced. Comparing with the results using the one stage NN model, the errors in *z*- and *xy*-directions are reduced by 27.9% and 37.8% respectively.

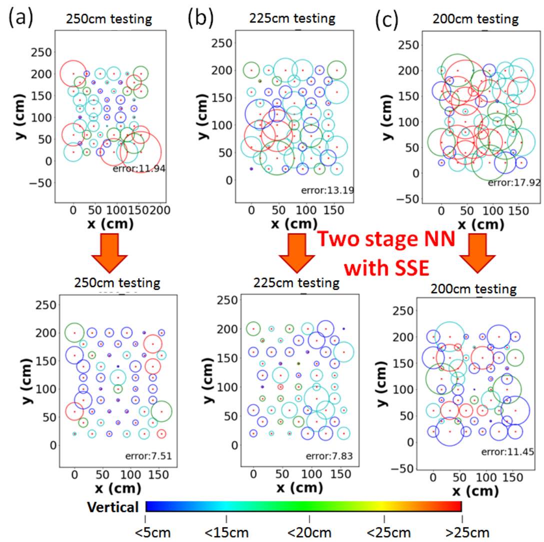

Fig. 4: Experimental average error distributions of the testing points using one stage NN and TSNN with SSE at (a)250 cm, (b)225 cm, (c)200 cm Rx planes.

Fig. 5 show the cumulative distribution function (CDF) of the measured positioning error using different NN models. When one stage NN model is used, the positioning error of 90% of the experimental data is within 24.2 cm; while using the TSNN model without and with the SSE, the errors are within 21.7 cm and 15.3 cm respectively. Hence, at the CDF at 90% positioning error, the TSNN model with SSE can reduce the errors by 36.8% when compared with that in the one stage NN model.

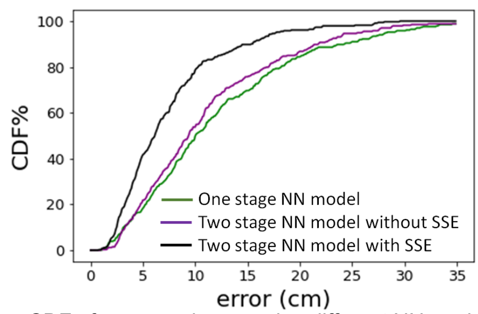

Fig. 5: CDF of measured error using different NN models.

Conclusions

We experimentally demonstrated a 3D VLP utilizing TSNN with SSE to mitigate the light non-overlapping regions. In a practical room of 200 × 150 × 300 cm^3, the average errors are <9 cm. The errors in *z*- and *xy*-directions were reduced by 27.9% and 37.8% respectively when compared with the one-stage NN without SSE.

Acknowledgements

We would like to acknowledge the Ministry of Science and Technology, Taiwan (MOST-110-2221-E-A49-057-MY3, MOST-109-2221-E-009-155-MY3).

References

[1] H. L. Minh, D. O'Brien, G. Faulkner, L. Zeng, K. Lee, D. Jung, Y. Oh, and E. T. Won "100-Mb/s NRZ visible light communications using a postequalized white LED," *IEEE Photon. Technol. Lett.*, vol. 21, pp. 1063-1065, 2009.

[2] L. Grobe, A. Paraskevopoulos, J. Hilt, D. Schulz, F. Lassak, F. Hartlieb, C. Kottke, V. Jungnickel, and K. D. Langer, "High-speed visible light communication systems," *IEEE Comm. Mag.*, vol. 51, pp. 60-66, 2013.

[3] H. Haas, "LiFi is a paradigm-shifting 5G technology," *Reviews in Physics*, vol. 3, pp. 26-31, 2018.

[4] C. W. Chow, C. H. Yeh, Y. Liu, Y. Lai, L. Y. Wei, C. W. Hsu, G. H. Chen, X. L. Liao, and K. H. Lin, "Enabling techniques for optical wireless communication systems," *Proc. OFC 2020*, paper M2F.1 (Invited).

[5] T. Koonen, K. Mekonnen, F. Huijskens, N. Q. Pham, Z. Cao and E. Tangdiongga, "Optical wireless GbE receiver with large field-of-view," *Proc. ECOC*, 2021, pp. 1-4, doi: 10.1109/ECOC52684.2021.9606055.

[6] Y. Zhuang, L. Hua, L. Qi, J. Yang, P. Cao, Y. Cao, Y. Wu, J. Thompson, and H. Haas., "A survey of positioning systems using visible LED lights," *IEEE Comm. Surv. & Tut.*, vol. 20, pp. 1963-1988, 2018.

[7] C. Xie, W. Guan, Y. Wu, L. Fang, and Y. Cai, "The LED-ID detection and recognition method based on visible light positioning using proximity method," *IEEE Photon. J.*, vol. 10, pp. 7902116, 2018.

[8] P. F. Du, S. Zhang, C. Chen, A. Alphones, and W. D. Zhong, "Demonstration of a low-complexity indoor visible light positioning system using an enhanced TDOA scheme," *IEEE Photon. J.*, vol. 10, pp. 7905110, 2018.

[9] C. Y. Hong, Y. C. Wu, Y. Liu, C. W. Chow, C. H. Yeh, K. L. Hsu, D. C. Lin, X. L. Liao, K. H. Lin, and Y. Y. Chen, "Angle-of-arrival (AOA) visible light positioning (VLP) system using solar cells with third-order regression and ridge regression algorithms," *IEEE Photon. J.*, vol. 12, pp. 7902605, 2020.

[10] C. W. Hsu, J. T. Wu, H. Y. Wang, C. W. Chow, C. H. Lee, M. T. Chu, and C. H. Yeh, "Visible light positioning and lighting based on identity positioning and RF carrier allocation technique using a solar cell receiver," *IEEE Photon. J.*, vol. 8, pp. 7905507, 2016.

[11] S. Zhang, P. Du, C. Chen, W. D. Zhong, and A. Alphones, "Robust 3D indoor VLP system based on ANN using hybrid RSS/PDOA," *IEEE Access*, vol. 7, pp. 47769-47780, 2019.

[12] P. Du, S. Zhang, C. Chen, H. Yang, W. D. Zhong, R. Zhang, A. Alphones, and Y. Yang, "Experimental demonstration of 3D visible light positioning using received signal strength with low-complexity trilateration assisted by deep learning technique," *IEEE Access*, vol. 7, pp. 93986-93997, 2019.

[13] J. He, C. W. Hsu, Q. Zhou, M. Tang, S. Fu, D. Liu, L. Deng, and G. K. Chang, "Demonstration of high precision 3D indoor positioning system based on two-layer ANN machine learning technique," *Proc. OFC* 2019, Paper Th3I2.